

Environmental and Costs Analysis of Concrete and Ultra-high Performance (UHPC) Bridge Decks Subjected to Local Climate Effects

Jin Fan¹, Wei Huang², Hao Wang³, Matthew P. Adams⁴, Matthew J. Bandelt^{5,*}

¹ Department of Civil and Environmental Engineering, University of California, Davis, Davis, CA, 95616 USA; John A. Reif, Jr., Department of Civil and Environmental Engineering, New Jersey Institute of Technology, Newark, NJ, 07102, USA, jdfan@ucdavis.edu

² Department of Civil and Environmental Engineering, Rutgers, The State University of New Jersey, Piscataway, 08854, USA, wh288@scarletmail.rutgers.edu

³ Department of Civil and Environmental Engineering, Rutgers, The State University of New Jersey, Piscataway, 08854, USA, hw261@soe.rutgers.edu

⁴ John A. Reif, Jr., Department of Civil and Environmental Engineering, New Jersey Institute of Technology, Newark, NJ, 07102, USA, matthew.p.adams@njit.edu

⁵ John A. Reif, Jr., Department of Civil and Environmental Engineering, New Jersey Institute of Technology, Newark, NJ, 07102, USA, bandelt@njit.edu

Abstract

Ultra-high-performance concrete (UHPC) exhibits high compressive strength and good durability. However, owing to the dense microstructure of UHPC, carbonation curing cannot be performed to capture and sequester carbon dioxide (CO₂). In this study, CO₂ was added to UHPC indirectly. Gaseous CO₂ was first converted into solid calcium carbonate (CaCO₃) using calcium hydroxide, and the converted CaCO₃ was then added to UHPC at 2, 4, and 6 wt.% based on the cementitious material. The performance and sustainability of UHPC with indirect CO₂ addition were investigated through macroscopic and microscopic experiments. The experimental results showed that the method used did not negatively affect the performance of UHPC. Compared with the control group, the early strength, ultrasonic velocity, and resistivity of UHPC containing solid CO₂ improved to varying degrees. Microscopic experiments, such as heat of hydration and thermogravimetric analysis (TGA), demonstrated that adding captured CO₂ accelerated the hydration rate of the paste. Finally, the CO₂ emissions were normalized according to the compressive strength and resistivity at 28 days. The results indicated that the CO₂ emissions per unit compressive strength and unit resistivity of UHPC with CO₂ were lower than those of the control group.

Keywords: Ultra-high-performance concrete; Microstructure; CO₂ absorption.

1. Introduction and Background

Production of portland cement, the main contributor of CO₂ emissions from concrete production, currently exceeds 4 billion tons annually [1]. Consequently, concrete, the most widely used construction material, accounts for approximately 8% of global anthropogenic CO₂ emissions [2, 3]. In the midst of the growing climate crisis, the demand for construction materials is expected to grow due to trends in development, urbanization, and population growth [4]. With concrete consumption expected to grow, it is imperative to adapt the construction sector to prevent additional emissions.

In addition to climate challenges, maintenance and rehabilitation of critical infrastructure, such as highway bridges, present ongoing challenges for bridge owners and transportation agencies. These structures are subjected to constant traffic loads; and bridge decks, which are most commonly made of concrete, are subjected to harsh environmental conditions leading to deterioration over time [5]. To address these challenges, there is growing interest in exploring non-conventional building materials that can promote an environmentally sustainable and socially resilient built environment [6, 7].

Ultra-high performance concrete (UHPC) is one such revolutionary material that has demonstrated improved performance and longevity [8, 9, 5]. Compared to conventional concrete, UHPC exhibits superior resistance to cracking [10, 11] and harmful material ingress [12, 13], and is able to achieve significantly higher mechanical strength [14, 15] due to its dense microstructure and the incorporation of steel fibers [16, 17]. Although UHPC's mechanical [18, 19, 20, 21, 22] and durability performance [23, 24, 25, 26] have been extensively studied, its environmental impacts have received limited attention. At the material level, UHPC has higher environmental impacts than concrete due to the higher volume of portland cement and steel fibers [27]. However, due to UHPC's high mechanical strength, UHPC structures can reduce material volume and thus reduce carbon emissions by up to 36.6%, as demonstrated by Joe and Moustafa [28]. Similarly, Sameer et al. [29] indicated that UHPC bridge design could lower the carbon footprint of the bridge by 14% compared to reinforced concrete bridges. In contradiction, studies by Stengel and Schießl [30] and M'arquez et al. [31] showed that the adoption of UHPC material did not produce a more environmentally friendly bridge construction, despite a significant reduction in the volume of materials. Meanwhile, beyond the construction stage, UHPC structures could have lower carbon emissions compared to conventional concrete structures when considering the use and maintenance stage. For example, Dong [32] found that a UHPC girder had lower carbon emission compared to a concrete girder due to less frequent maintenance requirements over the same lifespan.

Among the limited studies that considered the maintenance stages of a structure's life cycle, even fewer have integrated life-cycle prediction analysis. This analysis is critical for determining life spans and thus accurately quantifying life cycle carbon emissions. The study by Fan et al. [33] predicted the lifespans of a set of UHPC beams through multi-physics modeling and found that UHPC's high mechanical strength and excellent durability performance resulted in 48% lower carbon emissions compared to conventional concrete beams when considering maintenance stages. However, the demolition stage and the allocation of waste materials to landfills also need to be quantified. Furthermore, none of those studies, except Stengel and Schießl [30] considered categories of environmental impacts other than carbon emission, such as air pollutants. The inconsistent quantification of carbon emissions from the construction stage, the lack of service life predictions, the limited investigation of cradle-to-grave life cycle analysis, and the insufficient quantification of environmental impacts suggest that a comprehensive study of whole-stage life cycle analysis, based on physics-informed models, is needed to better achieve sustainable and resilient design goals when adopting UHPC materials. In addition to carbon emissions, other environmental impacts such as air pollutants must also be considered to avoid additional health risks to the local community. Finally, life cycle costs must be investigated to address the economic concerns of UHPC structures. The external societal costs of climate damage, quantified by the social costs of carbon (SCC), remain unexplored for UHPC materials.

This study aims to quantify and compare the long-term serviceability characteristics, environmental impacts, and costs of a reinforced normal-strength concrete bridge deck and a redesigned, smaller-sized reinforced UHPC bridge deck. A time-dependent multi-physics modeling framework was employed [34] which integrates realistic regional environmental factors such as the periodic applications of de-icing salts and fluctuating temperatures to simulate the performance of the bridge decks over their service life. Chloride profiles and structural deterioration after corrosion are used to assess the service life performance of reinforced UHPC and reinforced concrete bridge decks. The environmental impacts from cradle to grave, including greenhouse gas (GHG) emissions, air pollutants of nitrogen oxides (NOX), sulfur oxides (SOX), volatile organic compounds (VOCs), particulate matter less than 10 μm (PM10) and particulate matter less than 2.5 μm (PM_{2.5}), and carbon monoxide (CO) were quantified. The life cycle costs, including SCC, of the reinforced concrete and reinforced UHPC bridge decks were compared.

2. Background of Reinforced Concrete Bridge Deck Deterioration

In cold regions, such as the case selected in this study, de-icing materials are regularly applied to melt snow on roads and bridges. Corrosion of reinforcement steel can initiate and propagate due to accumulation of de-icing materials, and eventually deteriorate reinforced concrete infrastructures, especially in bridge decks in locations with high traffic loading. It is noted that there are many deterioration mechanisms that can shorten the service life of reinforced concrete structures, only corrosion (the most common one) was considered. The fundamental background of corrosion is briefly introduced in the following subsections.

2.1. Chloride Transport

Chloride transport in sound cementitious materials is a diffusion process governed by Fick's second law [35]:

$$\frac{\partial C_{Cl}}{\partial t} = D_{Cl} \left(\frac{\partial^2 C_{Cl}}{\partial x^2} + \frac{\partial^2 C_{Cl}}{\partial y^2} \right) \quad (1)$$

where C_{Cl} (% mass of cementitious materials) is the chloride concentration in concrete, D_{Cl} (m^2/s) indicates the chloride diffusion coefficient, and t (seconds) is the diffusion time.

A common method used to account for the effect of cracking on chloride transport in cementitious materials is the smeared cracking modeling technique. In such models, discrete crack geometry is not explicitly modeled. Instead, higher chloride diffusion coefficients are integrated in the cracked zones. The nonlinear relationships between crack width and the reference chloride diffusion coefficients of concrete and UHPC materials have been empirically described in the literature by the following equations, respectively [36, 13]:

$$D_{\text{ref,C}} = \begin{cases} 2 \times 10^{-11}w - 4 \times 10^{-10}, 30\mu\text{m} \leq w \leq 80\mu\text{m} \\ 14 \times 10^{-10}, w > 80\mu\text{m} \end{cases} \quad (2)$$

$$D_{\text{ref,UHPC}} = \begin{cases} 4 \times 10^{-12}w - 3 \times 10^{-11}, 10\mu\text{m} \leq w \leq 80\mu\text{m} \\ 3 \times 10^{-10}, w > 80\mu\text{m} \end{cases} \quad (3)$$

where w is crack width (μm). The chloride diffusion coefficient under the influence of temperature fluctuation is:

$$D_{Cl} = D_{\text{ref}} \cdot f(T) \quad (4)$$

$f(T)$ is described as follows [37]:

$$f(T) = \exp \left[\frac{U}{R} \left(\frac{1}{T_{\text{ref}}} - \frac{1}{T} \right) \right] \quad (5)$$

where U is the activation energy (44.6 KJ/mol), R is the gas constant (8.3 J/mol), T_{ref} is the reference

temperature (293.2 K) of the measured diffusion coefficient, and T is the concrete/UHPC temperature [37]. The impact of cracking on oxygen penetration in concrete/UHPC is described as [38]:

$$D_{O_2}^{\text{crack}} = \begin{cases} D_{O_2}^{\text{sound}}, w \leq w_{cr} \\ D_{O_2}^{\text{sound}} \times (w/w_{cr})^3, w > w_{cr} \end{cases} \quad (6)$$

where $D_{O_2}^{\text{crack}}$ and $D_{O_2}^{\text{sound}}$ are the oxygen diffusion coefficients in cracked and sound areas, respectively.

w_{cr} is the critical crack width for the study and is assumed as 0.1 mm [39, 40, 38].

2.2. Corrosion Initiation

Cementitious materials, including concrete and UHPC, serve as barriers against de-icing materials that can cause corrosion in steel reinforcement. Corrosion occurs gradually over time once the concentration of such materials reaches a threshold level, known as the critical chloride content Cl_{crit} [41, 42].

2.3. Corrosion Propagation

Corrosion is an electrochemical process, in which the electrons are freed from the steel and then react with water and oxygen. The electrochemical potential ϕ (mV) distribution and electrical charge flow i (A/m²) are governed by Laplace's equation and Ohm's law, respectively [43, 44, 45]:

$$\nabla \cdot \left(\frac{1}{\rho} \nabla \phi \right) = 0 \quad (7)$$

$$i = -\frac{1}{\rho} \nabla \phi \quad (8)$$

The numerical polarization equation for the anodic reaction is [45]: [45]:

$$i_{\text{Fe}} = i_{\text{Fe}}^0 \exp \left(2.303 \frac{\phi - \phi_{\text{Fe}}^0}{\beta_{\text{Fe}}} \right) \quad (9)$$

The polarization equation of cathodic reaction is [45]:

$$i_{O_2} = \frac{i_{O_2}^0 \exp \left(2.303 \frac{\phi - \phi_{O_2}^0}{\beta_{O_2}} \right)}{1 + \frac{i_{O_2}^0}{i_L} \exp \left(2.303 \frac{\phi - \phi_{O_2}^0}{\beta_{O_2}} \right)} \quad (10)$$

i_{Fe}^0 and $i_{O_2}^0$ represent the anodic and cathodic exchange current density, respectively. ϕ_{Fe}^0 and $\phi_{O_2}^0$ are the anodic and cathodic equilibrium potentials, respectively. β_{Fe} is the anodic Tafel constant, and β_{O_2} denotes the cathodic Tafel constant. i_L refers to the limiting current density [46, 47].

3. Service Life Modeling

3.1. Service Life Modeling Procedure

A time-dependent multi-physics modeling approach, building on the authors' previous work [34], was used in this study to predict the service life performance of the reinforced concrete and reinforced UHPC bridge decks. The de-icing material penetration, corrosion propagation, and structural response were connected through multiple modeling platforms and time steps. First, the initial structural response under traffic loading was simulated using DIANA Version 10.5 [48]. The transport properties of concrete and UHPC were then updated and incorporated into the chloride penetration analysis using the software package COMSOL Multiphysics Version 5.4 [49]. Next, the corrosion propagation simulation calculated rust expansion thickness, which was applied as an additional displacement load alongside

traffic loading in the structural analysis. This iterative process was repeated for subsequent time steps. The reader is referred to Fan et al. [34] for further background on the modeling approach.

At each time step, the corroded area of the steel reinforcement and the cracking status of the concrete and UHPC were updated. The time intervals for the reinforced concrete and reinforced UHPC bridge deck were set to four months and five years, respectively. The larger time step for the reinforced UHPC specimen was adopted to maintain the balance between computing efficiency and modeling accuracy.

3.2. Bridge Deck Descriptions and Boundary Conditions

Figure 1(a) shows a representative cross-section design of a reinforced concrete bridge deck. The thickness of the reinforced concrete bridge deck was 250 mm. The top and bottom concrete cover was 63 mm and 25 mm, respectively. The reinforcement bar diameter was 19mm. The span length was 3300 mm and only half of the span was simulated due to the symmetrical geometry.

Sustained traffic load was simplified as displacements applied at midspan. The reinforced UHPC bridge deck was redesigned with a reduced depth of 125 mm, which resulted in a load capacity (145.1 kN) equivalent to that of the reinforced concrete bridge deck (142.3 kN). Additionally, the cover depth of the reinforced UHPC bridge deck was reduced to 25 mm. According to ACI 224 R, the allowable crack width for the tensile face of a reinforced concrete structure exposed to de-icing chemicals is 0.18 mm [50]. Thus, load within the service load range that resulted in a crack width of 0.18 mm was chosen as the initial condition for the reinforced concrete bridge deck, which was 41 kN. For the reinforced UHPC bridge deck, the initial crack width at the same loading level (41 kN) was 0.017 mm, which was one order of magnitude smaller than that of the reinforced concrete bridge deck.

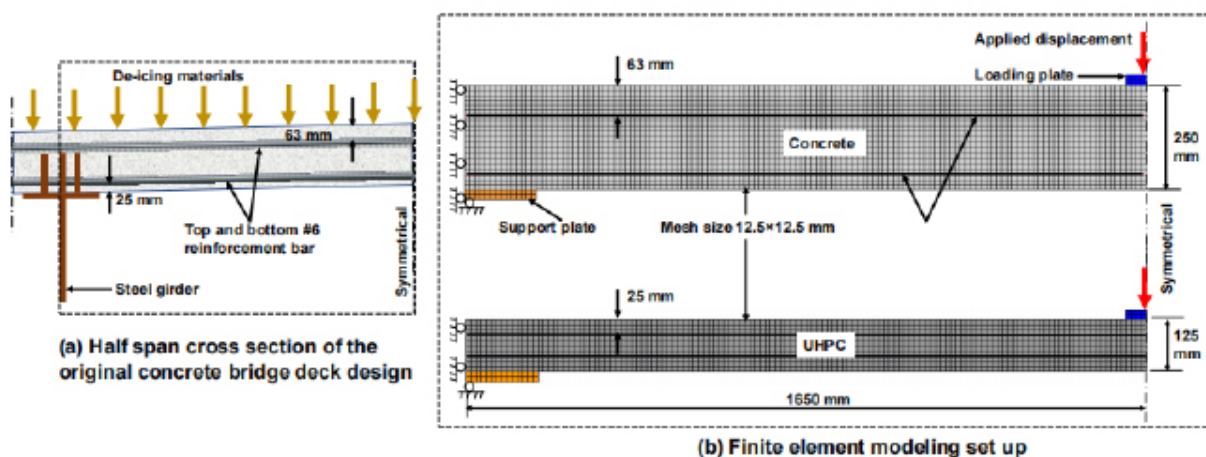


Figure 1: Concrete bridge deck and the finite element modeling (FEM) set up.

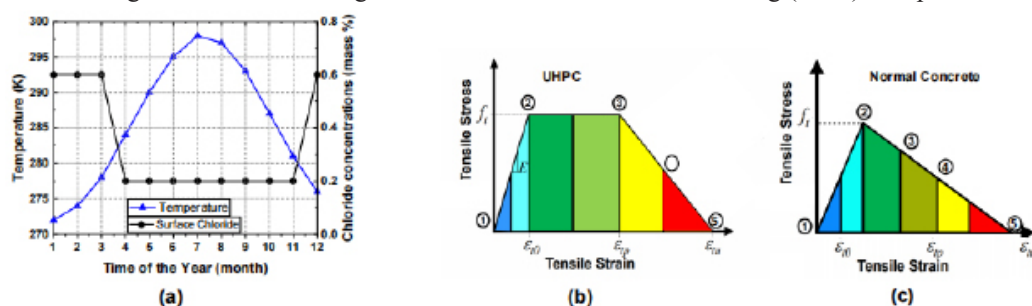


Figure 2: (a), Surface chloride conditions and temperature fluctuation; reference stress strain contour of (b) UHPC, and (c) concrete.

For bridges located in cold regions, de-icing materials used during the snowing seasons are the major

source of chloride ions. In this study, a steady and high concentration of chloride ions (0.6% of concrete/UHPC mass) was assumed to be applied at the top surface of the bridge deck for four months during the snow season. A lower residual surface chloride concentration of 0.2% of concrete/UHPC mass was assumed for the remainder of the year after the snow season [51]. Oxygen was assumed to be available at both the top and bottom sides. The seasonal variations in surface chloride content and local temperature fluctuations within the studied region are graphically presented in Figure 2(a) [51, 52].

3.3. Structural Response Modeling

Figure 1(b) shows the structural response modeling set up in DIANA Version 10.5 [48]. As shown in Figure 1(b), the left corner and left side deformation were restrained. A prescribed incremental displacement of 0.25 mm was applied at midspan to simulate the traffic loading. A total strainbased fixed-crack model with a shear retention factor of 0.01 was adopted to simulate the concrete and UHPC materials [53]. The mesh size of both concrete and UHPC was 7 mm \times 7 mm. The reinforcement bar was simulated as truss elements with the same mesh size. A line search algorithm and a secant Newton-Raphson scheme were selected for numerical convergence. The convergence criteria for energy, displacement, and force norms were 0.01%, 0.1% and 1%, respectively [11].

The mixture design of the concrete and UHPC bridge are shown in Table 1, the steel fiber volume of UHPC was 2%. The mechanical properties of normal strength concrete and UHPC were obtained from Shao and Billington [20] and are summarized in Table 2. Normal strength concrete had a tensile strength of 3.1 MPa with a tensile fracture energy of 0.144 MPa-mm, and a compressive strength of 41.9 MPa with a compressive fracture energy of 35.7 MPa-mm [20]. UHPC, on the other hand, had a tensile strength of 10.5 MPa and a tensile fracture energy of 11.2 MPa-mm, as well as a compressive strength of 185.8 MPa with a compressive fracture energy of 180.0 MPa-mm [20]. The reinforcing bar used in the study had a yielding strength of 455 MPa and an ultimate strength of 675 MPa [54].

Table 1: Mixture design and transport distances of raw materials to mixture plant (A2)

Materials	Unit	Concrete	UHPC	Unit	Rail	Truck	Ship
Glass Power	kg/m ²	0	26	ton-km	6	139	7
Silica Fume	kg/m ²	0	29	ton-km	6	139	7
Portland Cement	kg/m ²	106	89	ton-km	6	139	7
Fine Aggregate	kg/m ²	214	0	ton-km	21	54	14
Coarse Aggregate	kg/m ²	190	0	ton-km	26	39	11
Water	kg/m ²	57	14	ton-km	0	0	0
Silica Sand	kg/m ²	0	128	ton-km	26	39	11
Steel Bar	kg/m ²	42	27	ton-km	0	300	0
Steel Fiber	kg/m ²	0	20	ton-km	0	300	0
Steel Girder	kg/m ²	133	117	ton-km	0	300	0
Superplasticizer	kg/m ²	0	8	ton-km	0	300	0

3.4. Diffusion and Corrosion Modeling

Diffusion and corrosion modeling was completed in COMSOL Multiphysics Version 5.4 [49]. The impact of temperature on chloride transport was considered using the Equation (4). The oxygen ingress was considered to take place through both the top and bottom surfaces of the bridge deck in the computational model. On the other hand, chloride ion penetration was assumed to occur exclusively from the top surface, where de-icing material was applied.

Table 2: Mechanical properties of concrete, UHPC and steel

Mechanical properties	Notation	Unit	Concrete	UHPC	Steel
Tensile strength	f_t	MPa	3.1	10.5	-
Strain at crack initiation	ϵ_{t0}	%	0.01	0.019	-
Strain at onset of softening	ϵ_{tp}	%	0.01	0.2	-
Compressive strength	f'_c	MPa	41.9	185.8	-
Modulus of elasticity	E	GPa	31.2	53.5	200
Tensile fracture energy	G_f	MPa-mm	0.144	11.2	-
Compressive fracture energy	G_c	MPa-mm	35.7	180.0	-
Yield strength	f_y	MPa	-	-	455
Ultimate strength	f_u	MPa	-	-	675
Poisson's ratio	ν	mm/mm	0.2	0.18	0.30

The reference chloride transport coefficients for concrete and UHPC were reported as $D_{ref_c} = 1.3 \times 10^{-11} \text{ m}^2/\text{s}$ and $D_{ref_UHPC} = 4.5 \times 10^{-13} \text{ m}^2/\text{s}$, respectively [55]. The oxygen transport coefficients for concrete and UHPC were reported as $D_{O_2_c} = 3.02 \times 10^{-10} \text{ m}^2/\text{s}$ and $D_{O_2_UHPC} = 4.2 \times 10^{-10} \text{ m}^2/\text{s}$, respectively [55]. The electrical resistivity of concrete, ρ_c , was $159 \Omega \cdot \text{m}$, while the electrical resistivity of UHPC (ρ_{UHPC}) at the same level of saturation was $23067 \Omega \cdot \text{m}$ due to the dense material property [55,56]. The anodic Tafel slopes, $\beta_{Fe_c} = 65 \text{ mV/dec}$ and $\beta_{Fe_UHPC} = 61 \text{ mV/dec}$, as well as cathodic Tafel slopes $\beta_{O_2_c} = -138.6 \text{ mV/dec}$ and $\beta_{O_2_UHPC} = -130.9 \text{ mV/dec}$ were adopted from the literature [55]. The anodic equilibrium potential was set as $\phi_{j_{c3} \text{ hps13 } \backslash \text{o} \backslash \text{a} \backslash \text{l} \backslash \text{s} \backslash \text{u} \backslash \text{p} \text{ 30Fe}} = -600 \text{ mV}$, while the cathodic equilibrium potential was set as $\phi_{j_{c3} \text{ hps13 } \backslash \text{o} \backslash \text{a} \backslash \text{l} \backslash \text{s} \backslash \text{u} \backslash \text{p} \text{ 30O}_2} = 200 \text{ mV}$. The anodic and cathodic exchange current densities were $i_{j_{c3} \text{ hps13 } \backslash \text{o} \backslash \text{a} \backslash \text{l} \backslash \text{s} \backslash \text{u} \backslash \text{p} \text{ 30Fe}} = 2.75 \times 10^{-4} \text{ A/m}^2$ and $i_{j_{c3} \text{ hps13 } \backslash \text{o} \backslash \text{a} \backslash \text{l} \backslash \text{s} \backslash \text{u} \backslash \text{p} \text{ 30O}_2} = 6 \times 10^{-6} \text{ A/m}^2$, respectively [55]. In this study, a constant Cl_{crit} equal to 0.06% of concrete/UHPC mass is assumed [57, 58]. Surface oxygen concentration $O_{2surf} = 0.268 \text{ mol/m}^3$ [39], chloride diffusion activation energy $U = 44.6 \text{ KJ/mol}$, gas constant $R = 8.3 \text{ J/mol}$, and reference temperature $T_{ref} = 293.2 \text{ K}$. Detailed descriptions of the input parameters can be found in the authors' previous work [34].

After obtaining corrosion current density from corrosion modeling, the cross section loss and rust expansion was calculated [45, 59, 34] :

$$\sigma(t) = \frac{\int_0^t i_{corr}(t) dt \cdot M_s}{Z_{Fe} \cdot F \cdot \rho_s} \quad (11)$$

where t is the corrosion time (seconds), $M_s = 55.85 \text{ g/mol}$ is the atomic mass of iron, $Z_{Fe} = 2$ is the valency of the anodic reaction, and $\rho_s = 7800 \text{ kg/m}^3$ is the steel density.

The formation of corrosion products (rust) can occupy a greater volume than the original steel.

As a result, after part of the corrosion products fill the steel concrete interface, further accumulation of these products at the steel concrete interface can generate internal pressure on the steel and concrete. The thickness of the rust layer expansion can then be calculated using the following equation:

$$u(t) = (n - 1)\sigma(t) \quad (12)$$

where n is the volume expansion ratio of rust to steel and is assumed to be 3 in this study [60, 39, 42, 34]. Rust deformation was neglected in this analysis [61].

4. Environmental Impacts Analysis and Life-cycle Costs

4.1. Environmental Impact Analysis Scope

An attributional life cycle assessment (ALCA)—focusing on the directly attributable environ-

mental impacts over the product's full life cycle, was applied to the cradle-to-grave approach, in which emissions were assessed from raw material acquisition (sourcing, processing), construction (batching, pumping, curing), maintenance, and end-of-life through the grave (demolition, disposal of waste material). Transport-associated impacts were also considered.

A declared unit of 1 m^2 of reinforced concrete/UHPC were considered to determine life cycle inventories (LCI). In this study, carbon dioxide (CO_2), methane (CH_4), and nitrous oxide (N_2O) and their impacts were consolidated into CO_2 -equivalent ($\text{CO}_{2\text{-eq}}$) emissions to analyze GHG emissions, based on the 100-year global warming potentials [62]. The air pollutant emissions of nitrogen oxides (NO_x), sulfur oxides (SO_x), volatile organic compounds (VOC_s), carbon monoxide (CO), particulate matter less than $10 \mu\text{m}$ (PM_{10}), and particulate matter less than $2.5 \mu\text{m}$ ($\text{PM}_{2.5}$) were also quantified.

4.2. Environmental Impact Inputs and Assumptions

Emission factors of the life cycle stages are shown in Table 3. The emission factors of the raw materials (A1) were adopted from an open source tool, OpenConcrete, by Kim et al. [63]. Emission factors of steel girder and superplasticizer were adopted from Ecoinvent 3 database version 3 (a commonly used LCI database). Producing steel fiber and steel bar requires additional processing compared to that of a steel girder, therefore higher emission factors were assumed for steel fiber and steel bar. A2 is the raw material transport stage, the associated emission factors were based on US national average transport distances of rail, truck, and ship, according to Nahlik et al. [64]. The transport distances and modes of regular concrete constituents, steel, and admixture are shown in Table 1. The transport distances of glass powder, silica fume, PC, and aggregates were adopted from Marceau et al. [65]. Steel materials and superplasticizer were assumed to be transported with a distance of 300 km. For batching one cubic meter of UHPC, 0.35 liter of oil and 7.1 kWh of electricity were used while batching the same amount of concrete consumed 0.35 liter of oil and 4.4 kWh of electricity [29]. The emission factors of electricity is based on New Jersey electricity grid of US. Mixed concrete and UHPC were assumed to be transported (A4) 300 km to the construction site by truck within New Jersey. According to Sameer et al. [29], pumping of one cubic meter of concrete or UHPC consumed 2.7 kWh. Demolition of one cubic meter of concrete consumed 0.76 liter of oil and 18.3 kWh of electricity while demolition of the same amount of UHPC consumed 2 liters of oil and 36.5 kWh of electricity. Transport distance of the demolished waste to the landfill site (C2) was assumed to be 100 km. For the declared unit of 1 m^2 bridge deck, the volume of concrete and UHPC were 0.25 m^3 and 0.125 m^3 , respectively.

Table 3: Life cycle stages and emissions data

Life cycle stages	Materials/Processes	Unit	kg GHG	kg CO ₂	kg CH ₄	kg N ₂ O	kg NO _x	kg SO _x	kg PM ₁₀	kg PM _{2.5}	kg VOC	kg CO
A1	Glass Powder	per kg	5.53E-02	5.51E-02	2.52E-06	4.55E-07	4.18E-05	5.79E-05	2.11E-05	1.31E-05	1.90E-06	5.15E-05
A1	Silica Fume	per kg	0.00E+00	0.00E+00	0.00E+00	0.00E+00	0.00E+00	0.00E+00	9.30E-06	9.30E-06	0.00E+00	0.00E+00
A1	PC	per kg	9.50E-01	9.47E-01	4.02E-05	6.44E-06	3.37E-04	2.65E-03	4.46E-04	3.69E-04	1.03E-05	6.16E-04
A1	Fine Aggregate	per kg	2.07E-03	2.06E-03	9.00E-08	1.70E-08	1.56E-06	2.17E-06	1.17E-04	1.17E-04	7.10E-08	1.93E-06
A1	Coarse Aggregate	per kg	3.16E-03	3.15E-03	1.40E-07	2.60E-08	2.39E-06	3.31E-06	1.19E-04	1.18E-04	1.08E-07	2.95E-06
A1	Water	per kg	0.00E+00	0.00E+00	0.00E+00	0.00E+00	0.00E+00	0.00E+00	0.00E+00	0.00E+00	0.00E+00	0.00E+00
A1	Silica Sand	per kg	5.53E-02	5.51E-02	2.52E-06	4.55E-07	4.18E-05	5.79E-05	2.11E-05	1.31E-05	1.90E-06	5.15E-05
A1	Steel Bar	per kg	1.81E+00	1.81E+00	1.05E-02	3.23E-05	4.73E-03	4.49E-03	2.73E-03	2.66E-03	1.46E-02	2.39E-02
A1	Steel Fiber	per kg	1.81E+00	1.81E+00	1.05E-02	3.23E-05	4.73E-03	4.49E-03	2.73E-03	2.66E-03	1.46E-02	2.39E-02
A1	Steel Girder	per kg	9.06E-01	9.06E-01	5.25E-03	1.62E-05	2.37E-03	2.24E-03	1.37E-03	1.33E-03	7.32E-03	1.20E-02
A1	Superplasticizer	per kg	4.64E-01	4.64E-01	3.27E-05	1.69E-05	1.48E-03	2.75E-03	1.69E-04	8.35E-05	4.15E-05	8.81E-04
A2	Transport, rail	per ton-km	1.40E-02	1.40E-02	0.00E+00	0.00E+00	1.10E-04	3.96E-05	8.50E-07	2.89E-06	9.33E-06	3.88E-05
A2	Transport, truck	per ton-km	8.65E-02	8.65E-02	0.00E+00	0.00E+00	5.05E-04	5.20E-07	1.91E-05	1.50E-05	2.83E-05	9.23E-05
A2	Transport, ship	per ton-km	1.80E-03	1.80E-03	0.00E+00	0.00E+00	5.80E-05	1.27E-05	9.33E-06	2.53E-06	1.93E-06	3.75E-06
A3	Batching Concrete	per m ³	2.41E+00	2.40E+00	9.98E-05	1.81E-05	1.59E-03	1.62E-03	2.81E-04	6.97E-05	5.10E-05	1.36E-03
A3	Batching UHPC	per m ³	3.27E+00	3.25E+00	1.39E-04	2.51E-05	2.24E-03	2.52E-03	4.43E-04	1.08E-04	8.03E-05	2.16E-03
A4	Transport, truck	per ton-km	8.65E-02	8.65E-02	0.00E+00	0.00E+00	5.05E-04	5.20E-07	1.91E-05	1.50E-05	2.83E-05	9.23E-05
A5	Pumping (electricity)	per MJ	8.92E-02	8.89E-02	4.06E-06	7.33E-07	6.75E-05	9.35E-05	1.69E-05	4.02E-06	3.06E-06	8.31E-05
A5	Curing (oil)	per MJ	7.22E-02	7.20E-02	2.56E-06	4.69E-07	3.77E-05	9.82E-06	7.81E-07	4.12E-07	1.61E-07	2.87E-06
C1	Demolition (oil)	per MJ	7.22E-02	7.20E-02	2.56E-06	4.69E-07	3.77E-05	9.82E-06	7.81E-07	4.12E-07	1.61E-07	2.87E-06
C2	Transport (truck)	per ton-km	8.65E-02	8.65E-02	0.00E+00	0.00E+00	5.05E-04	5.20E-07	1.91E-05	1.50E-05	2.83E-05	9.23E-05
C3	Crushing Concrete	per m ³	3.78E+00	3.76E+00	1.50E-04	2.73E-05	2.33E-03	2.00E-03	3.32E-04	8.56E-05	6.07E-05	1.60E-03
C3	Crushing UHPC	per m ³	7.55E+00	7.53E+00	3.00E-04	5.47E-05	4.71E-03	4.00E-03	6.65E-04	1.71E-04	1.21E-04	3.21E-03

4.3. Social Impacts Analysis

In this study, SCC is evaluated as a theoretical measure that accounts for the multifaceted impacts of climate change. These include changes in agricultural productivity, health-related effects, property damage caused by flooding and extreme weather events, disruptions to energy infrastructure, heightened risks of conflict, climate-induced migration, and the economic value of ecosystem services [66]. The SCC and GHG emissions of concrete and UHPC bridge decks are applied to explore how incorporating externalized costs into market pricing might influence the relative differences between these mixtures. The externalized climate costs vary depending on the specific type of greenhouse gas (e.g., CO₂, CH₄, N₂O) and the timing of emission changes. In this analysis, the social costs of CO₂, CH₄, and N₂O are assumed to be \$116, \$3,800, and \$45,000, respectively, using a 2.5% discount rate [66].

4.4. Life-cycle Costs Analysis Methodology

Life cycle cost assessment (LCCA) is an effective method to evaluate the accumulated cost of managing a facility or processing a project with flexibility and comprehensiveness. The LCCA can be used to assess all significant and relevant costs over the service life cycle of a bridge deck, helping to optimize bridge deck designs that will implement the project objective at the lowest budget while with satisfied service level and performance.

The total cost of a bridge deck during its service life is mainly constituted of those from stages and activities such as initial construction, routine inspection, maintenance, demolition and recycling, which can be expressed as [67]:

$$LCC_{NPV} = C_{ic} + \sum_{i=1}^{n_{ri}} \frac{C_{ri}}{(1+r)^{t_i}} + \sum_{k=1}^{n_{mt}} \frac{C_{mt}}{(1+r)^{t_k}} + \frac{C_d}{(1+r)^T} - \frac{R_v}{(1+r)^T} \quad (13)$$

where LCC_{NPV} is the total cost represented by Net Present Value (NPV); r is the monetary discount rate; C_{ic} , C_{ri} , C_{mt} , C_d and R_v are costs of different activities: initial construction, routine inspection, maintenance, demolition and residual value, respectively; n_{ri} and n_{mt} are number of corresponding activities during the investigated period; T is the investigated service life.

4.5. Life-cycle Costs Inputs and Assumptions

The life cycle costs of the concrete and UHPC bridge decks were analyzed based on the results of the time-dependent multi-physics modeling. The investigated life period is 100 years considering the accumulated costs from initial construction, routine inspection, minor maintenance, major maintenance, and deck overlay. The costs from end of life such as demolition and recycling are not considered for a comparative analysis of the two types of bridge decks. The assessed dimension of the bridge deck follows the dimensional set up of FEM model, in which the thickness of concrete and UHPC decks are 250 mm and 125 mm, respectively, with both 1 lane width (3.7 m travel lane) and 1 mile length (1.6 km). It is assumed that the same traffic conditions are applied on these two bridges and the costs from traffic delay due to road closure for maintenance are not considered.

The initial construction and replacement costs of the concrete bridge deck are set as \$1,000/m² [68]. The unit costs of major and minor maintenance are set as \$500 and \$20 per square meter, respectively [68]. The routine inspection consists of observations and measurements needed to determine the physical and functional condition of the bridge. Minor maintenance is considered as preventive action before major maintenance (repair) [32, 33]. The unit cost of inspection is set as \$2/m² [68].

As for the bridge deck made with UHPC, related literature indicated that the material cost of UHPC is about 4 times of conventional concrete [32,69,33], and the thickness of UHPC deck can be much thinner owing to the advantages of high strength and reliable durability of UHPC [70], which is in accordance with the dimension set up in this study. Therefore, the normalized unit initial cost of UHPC bridge deck can be set as \$2,000/m², which is 2 times than that of RC bridge deck considering the thinner thickness of UHPC. The costs of minor maintenance and routine inspection for UHPC bridge deck are assumed to be the same as those

of RC bridge deck.

5. Results

This section presents the results of chloride content distribution and bridge deck deterioration, with a focus on comparing the findings between the reinforced concrete bridge deck and the reinforced UHPC bridge deck. The investigation includes the service life span, considering factors such as reinforcing bar cross-section loss, damage ratings of the cementitious materials, and the progression of cracking over time due to chloride exposure. Additionally, environmental impacts and life cycle costs, including social costs, were calculated based on the anticipated service life span. Figure 2(b) and (c) illustrates the reference contours of principal tensile strains for UHPC and concrete, serving as a measure of the level of cracking in the respective materials.

5.1. Chloride Profiles

Figure 3 (a)-(d) shows the comparative results of chloride distribution and cracking level following 30 years of chloride exposure under sustained traffic loading for both the reinforced concrete and reinforced UHPC bridge decks. As depicted in Figure 3, it is evident that the reinforced concrete bridge deck experienced significantly faster chloride ingress compared to the reinforced UHPC bridge deck under the same initial load condition. Additionally, the corrosion level in the reinforced concrete bridge deck reached 100% for the top reinforcing bar, whereas the reinforced UHPC bridge deck exhibited only 13.3% of the top reinforcing bar corrosion, despite having a concrete cover that was 2.52 times thicker than that of UHPC. The simulation results also indicate that corrosion initiation in the reinforcing bars of the reinforced concrete bridge deck occurred after one year, whereas in the reinforced UHPC bridge deck, it was 25 years. This notable difference can be attributed to the combined effect of slow chloride transportation and enhanced cracking resistance provided by UHPC beams. The simulation results, particularly in terms of chloride profiles, further verify the exceptional corrosion resistance of UHPC material.

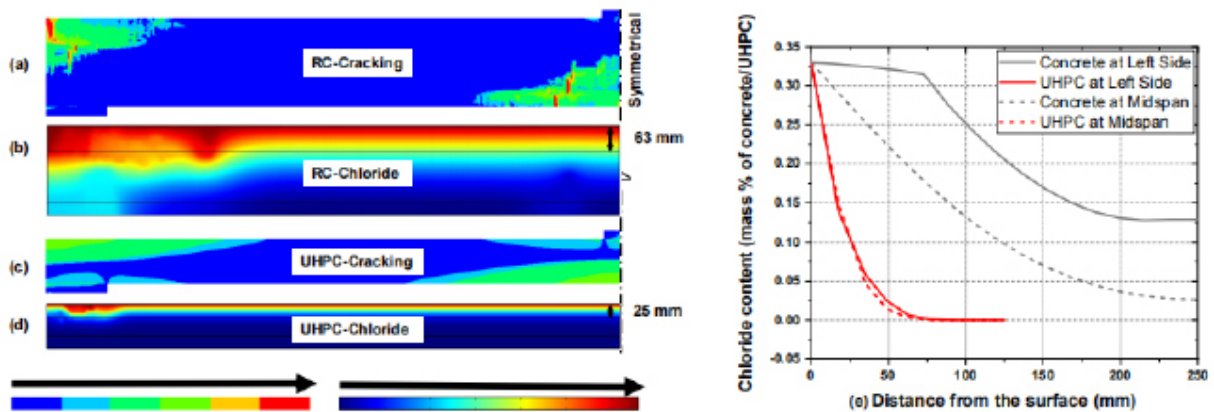


Figure 3: Damage patterns, chloride contours, and chloride profile.

Figure 3(e) provides additional insights into the chloride profiles at different depths of the bridge decks, specifically at the left side and midspan. It is observed that cracks predominantly occurred at the left side of the top surface when the traffic load was applied at midspan. Consequently, larger crack widths and a higher number of cracks were present on the left side of the top surface, where chloride was applied, leading to accelerated chloride transport on the left side of the reinforced concrete bridge deck. As a result, chloride concentrations were significantly higher on the left side of the concrete bridge deck. However, minimal variations in chloride profiles were observed across different horizontal locations of the reinforced UHPC bridge deck. This can be attributed to the multiple fine cracks along the horizontal direction, as shown in Figure 3(d). These findings emphasize the importance of crack distribution and width in determining the extent

of chloride transport, highlighting the superior crack resistance and corrosion protection capabilities of UHPC compared to traditional reinforced concrete structures.

5.2. Bridge Decks Deterioration

5.2.1. Steel cross-section loss

The corrosion-induced deterioration of the steel reinforcement bars in infrastructure is a critical concern, and assessing the extent of cross-section loss provides valuable insights into the long-term durability of bridge decks. After 30 years of exposure to chloride, the steel reinforcement bars in the reinforced concrete bridge deck exhibited a significant cross-section loss of 12%. This substantial degradation highlights the vulnerability of traditional reinforced concrete structures to corrosion-related damage over extended periods. In contrast, the reinforced UHPC bridge deck demonstrated exceptional resistance to corrosion-induced deterioration. Even after an extended exposure period of 140 years, the steel reinforcement bars in the UHPC deck experienced a comparatively minimal cross-section loss of only 5.3%. The differences in cross-sectional loss between the reinforced UHPC bridge deck and the reinforced concrete bridge deck can be attributed to the notable difference in corrosion propagation rates. This outstanding performance underscores the effectiveness of UHPC in mitigating chloride penetration and protecting the embedded steel from corrosion-induced degradation over the prolonged service life.

5.2.2. Concrete and UHPC damage ratings

The material deterioration of concrete and UHPC can be measured using a rating measurement based on the extent of the damaged area [71]:

$$R = A \times 100 + B \times 70 + C \times 40 + D \times 0 \quad (14)$$

A, B, C, and D represent the percentage area of the materials classified as being in sound, fair, poor, and severe damage conditions, respectively. An A rating of 0 indicates worst condition, while a rating of 100 indicates best condition. The damage level of the concrete and UHPC materials can be determined by referring to the reference principal strain contours of the finite elements, as illustrated in Figure 2(b) and (c). For instance, when the principal tensile strain fell within the range of 1 to 2, the concrete and UHPC were considered to be in a sound condition as the materials were still within the elastic range. In the range of 2 to 3, micro-cracking in UHPC began to develop, which was classified as a fair condition. The poor condition and severe damage in UHPC were assumed when the principal tensile strain ranged from 3 to 4 and from 4 to 5, respectively. Conversely, normal strength concrete was assumed to exhibit fair damage in the range of 2 to 3, while the ranges of 3 to 4 and 4 to 5 were associated with poor and severe damage, respectively.

The reinforced concrete bridge deck exhibited a deterioration rating of 79.1% after 30 years of chloride exposure, whereas the reinforced UHPC bridge deck demonstrated a significantly higher rating of 92.8% after 140 years of chloride exposure. The higher damage resistance of UHPC can be attributed to the synergistic effect of the dense material properties and the inherent cracking resistance of UHPC.

5.2.3. Cracking development

To assess the extent of cracking in the bridge decks, the crack density was determined by calculating the ratio of the total cracked area to the measured area. Over time, the cracks in both bridge decks exhibited an increase in length and width, influenced by factors such as traffic load and the expansion of corrosion products following chloride exposure. Figure 4 illustrates the crack density and number of cracks in the bridge decks. The cracking density was calculated as the total length of cracks over the measured area [72]. To measure the crack density, a smaller crack width of 0.01 mm was chosen for the reinforced UHPC bridge deck, while a width of 0.05 mm was selected for the reinforced concrete bridge deck, considering the micro-cracking characteristics of UHPC. The selection of different crack widths in the modeling process was based on the ability of the computational model to capture the distinct crack behavior of UHPC and normal strength concrete materials. UHPC is known for its unique microstructure and enhanced ductility, which can result

in smaller crack widths compared to normal strength concrete. In the modeling of UHPC, a smaller crack width of 0.01 mm was chosen to accurately represent the microcracking characteristics and improved crack resistance of this material. On the other hand, normal strength concrete typically exhibits larger crack widths under similar loading conditions. In the modeling of normal strength concrete, a crack width of 0.05 mm was selected to represent the typical behavior of this material.

As shown in Figure 4, both the reinforced concrete and the reinforced UHPC bridge decks exhibited 13 cracks after 30 years of chloride exposure. However, the cracking density of the reinforced UHPC bridge deck was 43.3% lower than the reinforced concrete bridge deck after 30 years of chloride exposure. This was attributed to the smaller crack depth in UHPC materials. The reinforced UHPC bridge deck reached the same level of cracking density after 140 years of chloride exposure.

These findings establish the significant advantage of using UHPC in bridge deck construction, particularly in chloride-rich environments. The exceptional durability exhibited by the reinforced UHPC bridge deck highlights its potential for long-lasting, sustainable infrastructure solutions. The superior corrosion resistance of UHPC offers the potential for reduced maintenance requirements and life-cycle costs, ensuring the longevity and structural integrity of bridge decks in challenging environmental conditions.

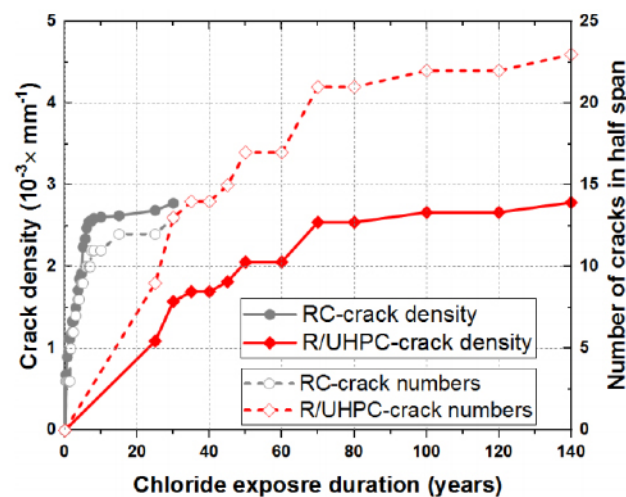


Figure 4: Number of cracks and cracking density over chloride exposure time.

5.3. Initial GHG Emissions and Air Pollutants

Figure 5 illustrates the average GHG emissions and air pollutants associated with the concrete and UHPC bridge decks per m^2 , covering the A1 to A5 life cycle stages. These stages include emissions from raw material acquisition, transportation, batching, pumping, and curing. The GHG emissions per m^2 of concrete and UHPC bridge deck were 345 kg and 326 kg $\text{CO}_{2\text{-eq}}$, respectively. Despite UHPC generally having higher GHG emissions during construction, due to its greater cement content and the addition of steel fibers [73], the GHG emissions for the UHPC bridge deck, based on the declared functional unit (1 m^2 bridge deck), were 6% lower than those of the concrete bridge deck. This reduction is attributed to the reduced volume of material required per m^2 : only 0.125 m^3 of UHPC is needed compared to 0.25 m^3 of concrete.

As shown in Figure 5, a similar trend is observed for air pollutants. NO_x and SO_x, which contribute to acid rain and smog formation, from UHPC bridge deck were 8% and 4% lower than that of the concrete bridge deck, respectively. The combined results of PM_{2.5} and PM₁₀, which are associated with respiratory and cardiovascular health risks, was 16% lower for the UHPC bridge deck. VOC and CO emissions, both contributors to air quality degradation, were both 3% lower for the UHPC bridge deck compared to the concrete bridge deck. These reductions demonstrate the environmental efficiency of UHPC, where its superior mechanical properties enable lower material use, offsetting the higher emissions of its components and resulting in a net improvement in sustainability.

5.4. Life Cycle GHG Emissions

Based on previous deterioration simulation results 5.2, the deck overlay and deck replacement are applied after 15 years and 60 years of service, respectively, for the RC bridge deck, and that minor maintenance is applied every 4 years after initial construction. It is assumed that the UHPC bridge deck is free of major maintenance and deck replacement necessary within the 100-year service life due to its superior performance in deterioration simulation, and its minor maintenance is applied every 4 years after 24 years of service when setting the crack density of $1 \times 10^{-3} \text{ mm}^{-1}$ as the threshold. Routine inspections are completed every 2 years for all types of bridge decks.

The UHPC bridge deck demonstrates significantly greater durability, requiring less maintenance and no replacement over an investigated period of 100 years. In contrast, the concrete bridge deck demands frequent maintenance, which adds to its environmental burden over its life cycle. Consequently, the life cycle GHG emissions of the UHPC bridge deck are substantially lower than those of the concrete bridge deck. As shown in Figure 6, the total GHG emissions from raw material acquisition (A1) to disposal and crushing (C3) are $2595 \text{ kg CO}_{2\text{-eq}} \text{ per m}^2$ for the concrete bridge deck and $952 \text{ kg CO}_{2\text{-eq}} \text{ per m}^2$ for the UHPC bridge deck, respectively. The GHG emissions from the maintenance stage (B1-B3) accounted for 86% and 65% of the total emissions for the concrete and UHPC bridges, respectively. A similar trend was observed for air pollutants. NO_x emissions during the maintenance stage constituted 86% and 65% of the total emissions for the concrete and UHPC bridges, respectively. SO_x emissions from maintenance were 87% and 65% of the total for the concrete and UHPC bridges, respectively. Particulate matter, including PM_{2.5} and PM₁₀, as well as (VOC_s), also accounted for 87% and 65% of the total emissions for the concrete and UHPC bridges, respectively. Similarly, CO emissions from the maintenance stage contributed 87% and 65% of the total emissions for the concrete and UHPC bridges, respectively. These results emphasize the significant environmental burden of the maintenance stage, particularly for the concrete bridge.

5.5. Life-cycle Costs

Figure 7 illustrates the life cycle costs of the concrete and UHPC bridge decks over a 100-year service life, including material, maintenance, construction, and social costs. At year 60, the total costs (comprising life cycle cost net present value, LCCNVP, and social costs) of the concrete bridge (\$14.8 million) surpassed those of the UHPC bridge (\$13.5 million). The lower total costs of the UHPC bridge after 60 years indicate its economic advantage, driven by reduced maintenance requirements, longer service life, and lower associated social costs. This demonstrates that, despite potentially higher initial costs, the UHPC bridge provides significant long-term cost savings and sustainability benefits. To assess the sensitivity of how initial material costs influence the total costs of bridge decks, various UHPC material costs (\$/m³) were considered. Specifically, UHPC material costs (\$/m³) were evaluated from two to six times the unit material cost of conventional concrete. Accordingly, the initial unit UHPC deck costs examined were \$1000/m², \$1500/m², \$2000/m², \$2500/m², \$3000/m². The resulting initial and total costs are summarized in Table 4. When the material cost of UHPC reaches five times that of concrete, the total cost of an UHPC bridge deck consistently exceeds that of a concrete bridge deck.

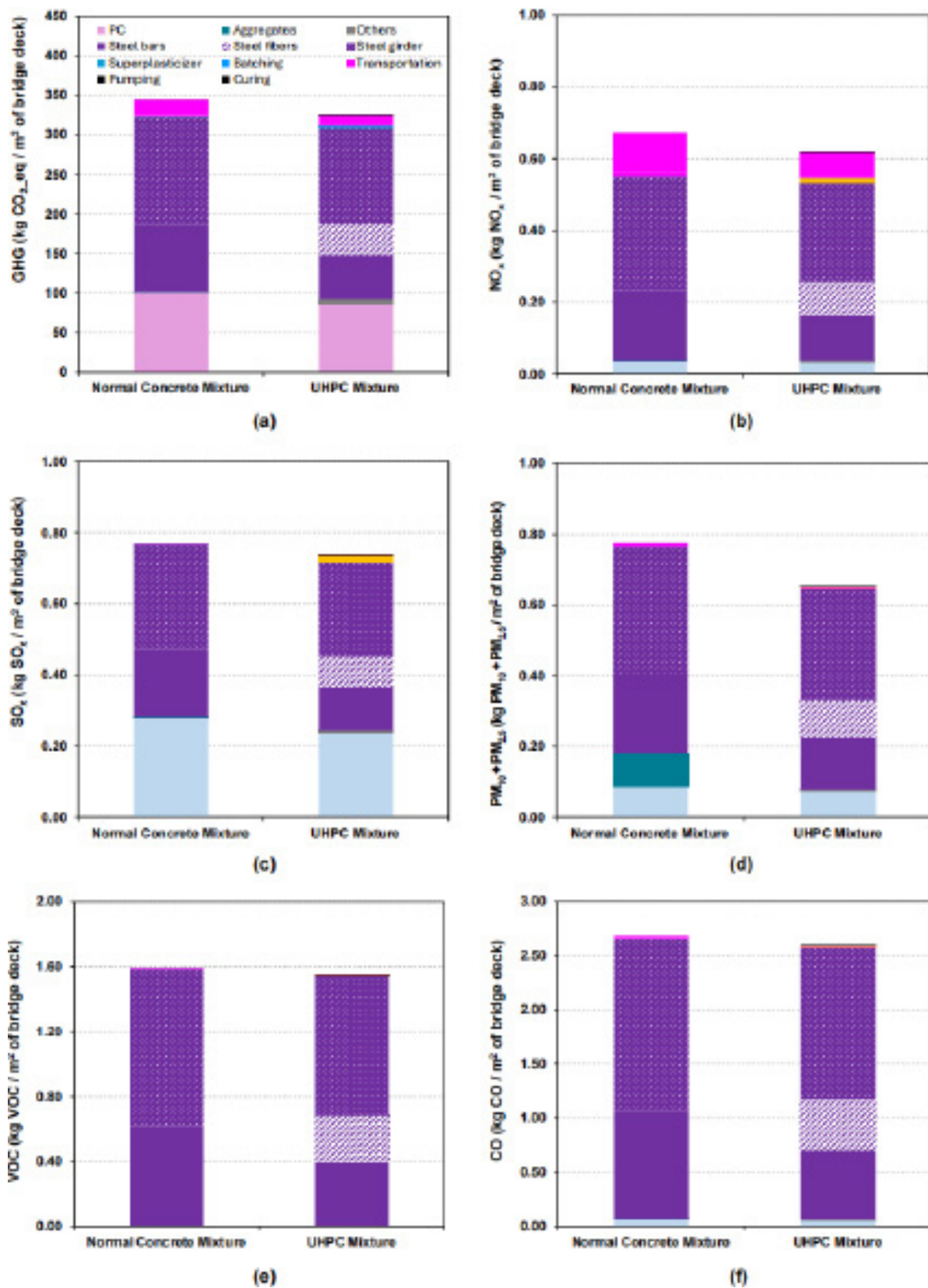


Figure 5: Emissions from A1-A5: (a) GHG emissions; (b) NO_x emission; (c) SO_x emission; (d) PM_{2.5} and PM₁₀ emissions; (e) VOC_s emission; (f) CO emission.

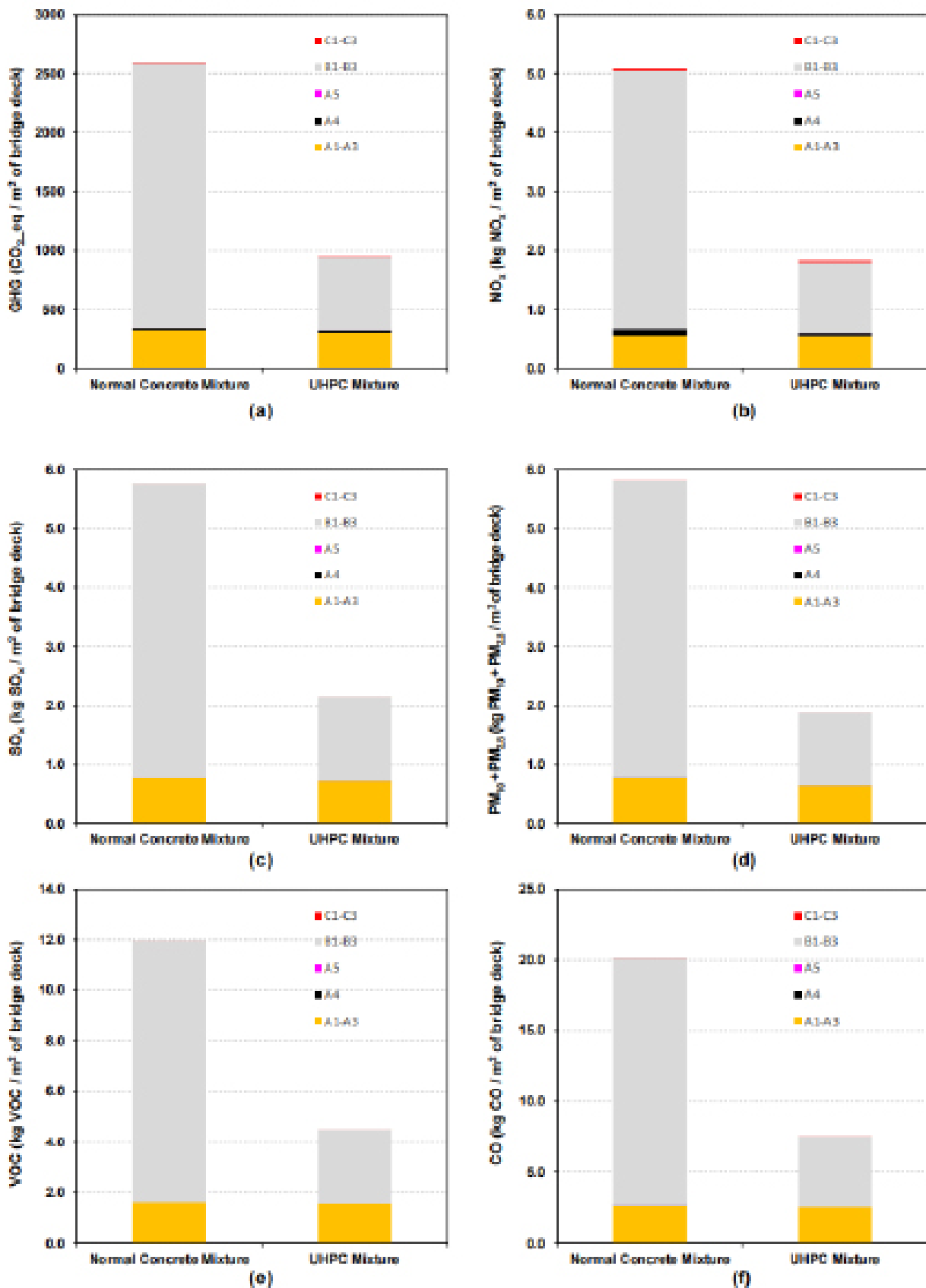


Figure 6: Life Cycle Emissions from A1-C3: (a) GHG emissions; (b) NO_x emission; (c) SO_x emission; (d) PM_{2.5} and PM₁₀ emissions; (e) VOC emission; (f) CO emission

Table 4: Cost Comparison Between Concrete and UHPC Bridge Decks

	Concrete			UHPC		
Initial Material Cost (\$/m ³)	4,000	8,000	12,000	16,000	20,000	24,000
Initial Unit Deck Cost (\$/m ²)	1000	1000	1500	2000	2500	3000
Total Cost at Year 60 (million \$/bridge deck)	14.8	6.9	10.4	13.5	16.8	20.1
Total Cost at Year 100 (million \$/bridge deck)	16.3	7.4	10.8	14.1	17.5	20.9

The social costs associated with the concrete and UHPC bridge over 100 years of service life were \$1.85 million and \$0.68 million, respectively. According to the Intergovernmental Panel on Climate Change (IPCC), while applying SCC has been effective in reducing GHG emissions, achieving net-zero GHG emissions by 2050 will require significantly higher carbon prices [74]. The SCC value of 116 USD per ton CO₂ used in this study is a conservative estimate [75]. There are studies suggest that the social cost of carbon could be as high as 1000 USD per ton CO₂ [76]. When higher SCC were to applied, the UHPC bridge showed greater benefits due to the lower life-cycle GHG emissions compared to that of the concrete bridge. If a lower discount rate (2%) were used, the social costs of the concrete and UHPC bridge would increase to \$2.85 million and \$1.04 million, respectively. These values highlight the potential for substantial variability in social cost estimates and underscore the importance of adopting an appropriate carbon price to drive meaningful emissions reductions.

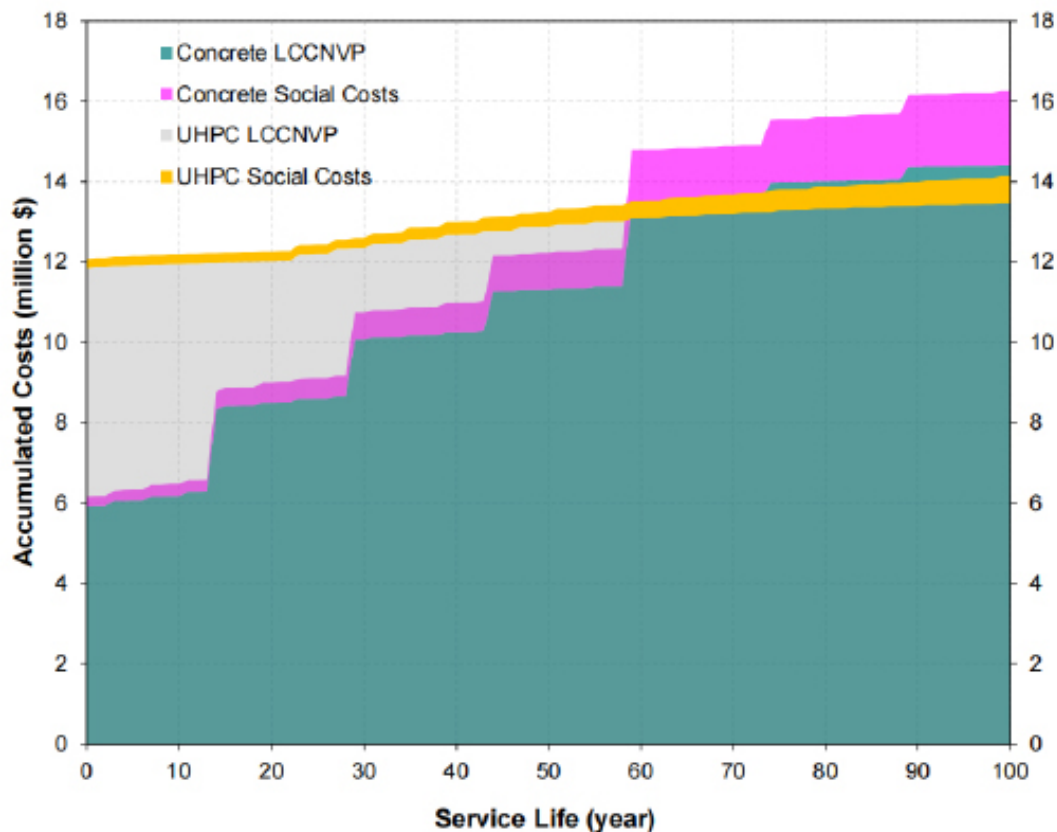


Figure 7: Life cycle GHG emission

6. Conclusions

This study compared reinforced concrete and ultra-high-performance concrete (UHPC) bridge decks over a 100-year service life, examining structural durability, environmental impacts, and life cycle costs under iden-



tical temperature fluctuations and exposure to de-icing materials. Results indicate that UHPC bridge decks offer superior performance across all evaluated metrics. The reinforced UHPC bridge deck demonstrated significantly slower structural deterioration, with reinforcing bar cross-section loss of only 5.3% after 140 years, compared to 12.0% for the reinforced concrete deck after just 30 years of exposure to chloride ingress. Similarly, UHPC decks exhibited higher resistance to damage and cracking, as evidenced by deterioration ratings of 92.8% and lower cracking densities even after extended service.

Environmental analysis revealed that the life cycle GHG emissions of the UHPC bridge deck were significantly lower, totaling 952 kg CO_{2-eq} per m² compared to 2595 kg CO_{2-eq} per m² for the concrete deck. This reduction was largely attributed to the UHPC's superior durability, which reduced maintenance-related emissions from stages B1 to B3, contributing 65% of total emissions for the UHPC bridge deck versus 86% for the concrete bridge deck. Comparable trends were observed for air pollutants, including nitrogen oxides (NO_x), sulfur oxides (SO_x), volatile organic compounds (VOC_s), particulate matter less than 10 μm (PM₁₀), and particulate matter less than 2.5 μm (PM_{2.5}), and carbon monoxide (CO). Ongoing research into lower-carbon UHPC systems, if successful, will result in even more reductions in the life-cycle carbon emissions [77, 78].

Economically, UHPC bridge decks demonstrated long-term cost advantages despite higher initial material costs. By year 60, the total costs of the reinforced concrete bridge deck, including net present value and social costs, exceeded those of UHPC decks (\$14.8 million vs. \$13.5 million). The substantial improvement in service life performance lead to cost savings in maintenance and repair expenses over time. Additionally, despite the potential higher initial construction costs associated with UHPC, the reduced bridge deck cross-section of the reinforced UHPC bridge deck can help offset some of these upfront expenses.

The findings of this study emphasize the potential of UHPC materials as a sustainable and cost-effective alternative to conventional concrete materials. By minimizing environmental impacts, reducing life cycle costs, and extending service life, UHPC provides a compelling solution for advancing sustainable infrastructure in the face of increasing environmental and economic challenges.

Acknowledgments

This material is based upon work supported by the New Jersey Department of Transportation through Contract ID 19-60155. Any opinions, findings, and conclusions or recommendations expressed in this material are those of the author(s) and do not necessarily reflect the views of the New Jersey Department of Transportation (NJDOT). The authors gratefully acknowledge financial support of NJDOT and the John A. Reif, Jr. Department of Civil and Environmental Engineering at New Jersey Institute of Technology.

References

- M. C. Summaries, et al., Mineral commodity summaries, US Geological Survey: Reston, VA, USA 200 (2021).
- C. IEA, et al., Technology roadmap low-carbon transition in the cement industry, France/WBCSD, Geneva, Switzerland. IEA, Paris (2018).
- S. A. Miller, A. Horvath, P. J. Monteiro, Readily implementable techniques can cut annual co2 emissions from the production of concrete by over 20%, *Environmental Research Letters* 11 (2016) 074029.
- J. A. Olsson, S. A. Miller, M. G. Alexander, Near-term pathways for decarbonizing global concrete production, *Nature Communications* 14 (2023) 4574.
- J. Fan, M. Adams, M. Bandelt, Service life prediction of RC and UHPC bridge decks exposed to regional environments, in: *International Interactive Symposium on Ultra-High Performance Concrete*, volume 3, Iowa State University Digital Press, 2023, p. 29.

- D.-Y. Yoo, S.-T. Kang, Y.-S. Yoon, Enhancing the flexural performance of ultra-high-performance concrete using long steel fibers, *Composite Structures* 147 (2016) 220–230.
- A. M. Tahwia, A. Essam, B. A. Tayeh, M. Abd Elrahman, Enhancing sustainability of ultra-high performance concrete utilizing high-volume waste glass powder, *Case Studies in Construction Materials* 17 (2022) e01648.
- X. Wang, D. Wu, J. Zhang, R. Yu, D. Hou, Z. Shui, Design of sustainable ultra-high performance concrete: A review, *Construction and Building Materials* 307 (2021) 124643.
- H. Kim, T. Koh, S. Pyo, Enhancing flowability and sustainability of ultra high performance concrete incorporating high replacement levels of industrial slags, *Construction and Building Materials* 123 (2016) 153–160.
- Z. B. Haber, I. De la Varga, B. A. Graybeal, B. Nakashoji, R. El-Helou, Properties and behavior of UHPC-class materials, Technical Report, United States. Federal Highway Administration. Office of Infrastructure . . . , 2018.
- Y. Shao, C.-C. Hung, S. L. Billington, Gradual crushing of steel reinforced HPFRCC beams: Experiments and simulations, *Journal of Structural Engineering* 147 (2021) 04021114.
- V. Perry, D. Zakariassen, First use of ultra-high performance concrete for an innovative train station canopy, *Concrete Technology Today* 25 (2004) 1–2.
- J. Fan, M. Adams, M. Bandelt, Multi-physics simulation of steel corrosion in reinforced UHPC beams under coupled sustained loading and chloride attack, in: *Computational Modelling of Concrete and Concrete Structures*, CRC Press, 2022, pp. 590–595.
- C.-C. Hung, S. El-Tawil, S.-H. Chao, A review of developments and challenges for uhpc in structural engineering: Behavior, analysis, and design, *Journal of Structural Engineering* 147 (2021) 03121001.
- B. Graybeal, E. Brühwiler, B.-S. Kim, F. Toutlemonde, Y. L. Voo, A. Zaghi, International perspective on UHPC in bridge engineering, *Journal of Bridge Engineering* 25 (2020) 04020094.
- C. Shi, Z. Wu, J. Xiao, D. Wang, Z. Huang, Z. Fang, A review on ultra high performance concrete: Part i. raw materials and mixture design, *Construction and Building Materials* 101 (2015) 741-751.
- P. Aghdasi, A. E. Heid, S.-H. Chao, Developing ultra-high-performance fiber-reinforced concrete for large-scale structural applications., *ACI Materials Journal* 113 (2016).
- C.-C. Hung, H.-H. Hung, Potential of sodium sulfate solution for promoting the crack-healing performance for strain-hardening cementitious composites, *Cement and Concrete Composites* 106 (2020) 103461.
- Y. Shao, S. Billington, Utilizing full UHPC compressive strength in steel reinforced UHPC beams, in: *International Interactive Symposium on Ultra-High Performance Concrete*, volume 2, Iowa State University Digital Press, 2019, pp. 1-9.
- Y. Shao, S. L. Billington, Impact of UHPC tensile behavior on steel reinforced uhpc flexural behavior, *Journal of Structural Engineering* 148 (2022) 04021244.
- M. Ye, L. Li, H. Li, C. Zhou, Shear behavior of joints in precast UHPC segmental bridges under direct shear loading, *Construction and Building Materials* 357 (2022) 129212.
- M. Ye, L. Li, D.-Y. Yoo, H. Li, X. Shao, C. Zhou, Mechanistic understanding of precast UHPC segmental beams with external tendons and epoxy joints subject to combined bending and shear, *Engineering Structures* 280 (2023) 115698.
- B. Graybeal, J. Tanesi, Durability of an ultrahigh-performance concrete, *Journal of materials in civil engineering* 19 (2007) 848-854.
- X.-g. Tang, Y.-j. Xie, G.-c. Long, Experimental study on performance of imitative rpc for sulphate leaching, *Journal of Asian Ceramic Societies* 4 (2016) 143-148.
- N. A. Soliman, A. Tagnit-Hamou, Using glass sand as an alternative for quartz sand in uhpc, *Construction and Building Materials* 145 (2017) 243-252.
- M.-G. Lee, Y.-C. Wang, C.-T. Chiu, A preliminary study of reactive powder concrete as a new repair material, *Construction and building materials* 21 (2007) 182-189.

- Y. Shi, G. Long, C. Ma, Y. Xie, J. He, Design and preparation of ultra-high performance concrete with low environmental impact, *Journal of Cleaner Production* 214 (2019) 633-643.
- C. D. Joe, M. Moustafa, Cost and ecological feasibility of using UHPC in bridge piers, in: *International Interactive Symposium on Ultra-High Performance Concrete*, volume 1, Iowa State University Digital Press, 2016, pp. 1-8.
- H. Sameer, V. Weber, C. Mostert, S. Bringezu, E. Fehling, A. Wetzel, Environmental assessment of ultra-high-performance concrete using carbon, material, and water footprint, *Materials* 12 (2019) 851.
- T. Stengel, P. Schießl, Life cycle assessment (lca) of ultra high performance concrete (UHPC) structures, in: *Eco-efficient construction and building materials*, Elsevier, 2014, pp. 528-564.
- J. M´arquez, D. Jauregui, B. Weldon, C. Newton, Potential environmental impact of using ultra-high performance concrete in simple, two and three-span continuous prestressed concrete bridges, in: *Bridge Maintenance, Safety, Management, Life-Cycle Sustainability and Innovations*, CRC Press, 2021, pp. 4076-4083.
- Y. Dong, Performance assessment and design of ultra-high performance concrete (UHPC) structures incorporating life-cycle cost and environmental impacts, *Construction and Building Materials* 167 (2018) 414-425.
- J. Fan, Y. Shao, M. J. Bandelt, M. P. Adams, C. P. Ostertag, Sustainable reinforced concrete design: The role of ultra-high performance concrete (uhpc) in life-cycle structural performance and environmental impacts, *Engineering Structures* 316 (2024) 118585.
- J. Fan, S. M. Shirkorshidi, M. P. Adams, M. J. Bandelt, Predicting corrosion in reinforced UHPC members through time-dependent multi-physics numerical simulation, *Construction and Building Materials* 340 (2022) 127805.
- J. Crank, *The mathematics of diffusion*, Oxford university press, London, UK, 1979.
- A. Djerbi, S. Bonnet, A. Khelidj, V. Baroghel-Bouny, Influence of traversing crack on chloride diffusion into concrete, *Cement and Concrete Research* 38 (2008) 877-883.
- A. V. Saetta, R. V. Scotta, R. V. Vitaliani, Analysis of chloride diffusion into partially saturated concrete, *Materials Journal* 90 (1993) 441-451.
- H.-W. Reinhardt, M. Jooss, Permeability and self-healing of cracked concrete as a function of temperature and crack width, *Cement and Concrete Research* 33 (2003) 981-985.
- C. Cao, 3D simulation of localized steel corrosion in chloride contaminated reinforced concrete, *Construction and Building Materials* 72 (2014) 434-443.
- J. Chen, W. Zhang, X. Gu, Modeling time-dependent circumferential non-uniform corrosion of steel bars in concrete considering corrosion-induced cracking effects, *Engineering Structures* 201 (2019) 109766.
- J. P. Broomfield, *Corrosion of steel in concrete: understanding, investigation and repair*, Taylor & Francis, New York, NY, USA, 2007.
- Y. Zhao, W. Jin, *Steel corrosion-induced concrete cracking*, Butterworth-Heinemann, Kidlington, Oxford, UK, 2016.
- J. Warkus, M. Raupach, J. Gulikers, Numerical modelling of corrosion–theoretical backgrounds, *Materials and Corrosion* 57 (2006) 614–617.
- S. Kranc, A. A. Sag˘u´es, Detailed modeling of corrosion macrocells on steel reinforcing in concrete, *Corrosion Science* 43 (2001) 1355–1372.
- H. B˘ohni, *Corrosion in reinforced concrete structures*, CRC Press LLC, Boca Raton, Florida, USA, 2005.
- R. W. Revie, *Corrosion and corrosion control: an introduction to corrosion science and engineering*, John Wiley & Sons, Hoboken, New Jersey, USA, 2008.
- E. Bardal, *Corrosion and protection*, Springer, London, UK, 2003.
- DIANA, *DIANA User’s Manual*, Delft, The Netherlands, 2022.
- COMSOL, *COMSOL Multiphysics Reference Manual*, Burlington, MA, USA, 2018.

- ACI Committee 224, Control of cracking in concrete structures, Technical Report, American Concrete Institute, 2001.
- M. M. Cheung, J. Zhao, Y. B. Chan, Service life prediction of rc bridge structures exposed to chloride environments, *Journal of Bridge Engineering* 14 (2009) 164–178.
- Climate-Data.org, Climate: New brunswick - climate graph, temperature graph, climate table, <https://en.climate-data.org/north-america/united-states-of-america/new-jersey/new-brunswick-1729/>, Accessed: 2022-12-17.
- P. Feenstra, J. Rots, A. Arnesen, J. Teigen, K. Hoiseth, A 3D constitutive model for concrete based on a co-rotational concept, in: *Computational Modelling of Concrete Structures. Proceedings of the Euro-C 1998 Conference on Computational Modelling of Concrete Structures*, Badgastein, Austria, 31 March-3 April, Brookfield, 1998, p. 13.
- M. J. Bandelt, S. L. Billington, Impact of reinforcement ratio and loading type on the deformation capacity of high-performance fiber-reinforced cementitious composites reinforced with mild steel, *Journal of Structural Engineering* 142 (2016) 04016084.
- A. Rafiee, Computer modeling and investigation on the steel corrosion in cracked ultra high performance concrete, Ph.d. dissertation, Kassel University, Kassel, Germany, 2012.
- J. Fan, M. Adams, M. J. Bandelt, Finite element simulation of mechanical-electrochemical coupling effects of steel corrosion in ecc structures, in: *2021 fib Symposium of Concrete Structures: New Trends for Eco-Efficiency and Performance*, fib. The International Federation for Structural Concrete, 2021, pp. 371–380.
- O. B. Isgor, A. G. Razaqpur, Modelling steel corrosion in concrete structures, *Materials and Structures* 39 (2006) 291–302.
- Y. Cao, C. Gehlen, U. Angst, L. Wang, Z. Wang, Y. Yao, Critical chloride content in reinforced concrete—an updated review considering chinese experience, *Cement and Concrete Research* 117 (2019) 58–68.
- A. Michel, B. J. Pease, A. Peterov'a, M. R. Geiker, H. Stang, A. E. A. Thybo, Penetration of corrosion products and corrosion-induced cracking in reinforced cementitious materials: Experimental investigations and numerical simulations, *Cement and Concrete Composites* 47 (2014) 75–86.
- C. Cao, M. M. Cheung, B. Y. Chan, Modelling of interaction between corrosion-induced concrete cover crack and steel corrosion rate, *Corrosion Science* 69 (2013) 97–109.
- C. Lu, W. Jin, R. Liu, Reinforcement corrosion-induced cover cracking and its time prediction for reinforced concrete structures, *Corrosion Science* 53 (2011) 1337–1347.
- J. G. Canadell, P. M. Monteiro, M. H. Costa, L. Cotrim da Cunha, P. M. Cox, A. V. Eliseev, S. Henson, M. Ishii, S. Jaccard, C. Koven, et al., Intergovernmental panel on climate change (ipcc). global carbon and other biogeochemical cycles and feedbacks, in: *Climate change 2021: The physical science basis. Contribution of working group I to the sixth assessment report of the intergovernmental panel on climate change*, Cambridge University Press, 2023, pp. 673–816.
- A. Kim, P. R. Cunningham, K. Kamau-Devers, S. A. Miller, Openconcrete: a tool for estimating the environmental impacts from concrete production, *Environmental Research: Infrastructure and Sustainability* 2 (2022) 041001.
- M. J. Nahlik, A. T. Kaehr, M. V. Chester, A. Horvath, M. N. Taptich, Goods movement life cycle assessment for greenhouse gas reduction goals, *Journal of Industrial Ecology* 20 (2016) 317-328.
- M. Marceau, M. A. Nisbet, M. G. Van Geem, Life cycle inventory of portland cement concrete, Portland Cement Association, 2007.
- Interagency Working Group on Social Cost of Greenhouse Gases, United States Government, Technical Support Document: Social Cost of Carbon, Methane, and Nitrous Oxide: Interim Estimates under Executive Order 13990, Technical Report, United States Government, 2021.
- D. M. Frangopol, Y. Dong, S. Sabatino, Bridge life-cycle performance and cost: analysis, prediction, optimisation and decision-making, in: *Structures and Infrastructure Systems*, Routledge, 2019, pp. 66-

84.

D. Cusson, Z. Lounis, L. Daigle, Benefits of internal curing on service life and life-cycle cost of high-performance concrete bridge decks-a case study, *Cement and Concrete Composites* 32 (2010) 339-350.

T. Ngo, Application of UHPC in Long Span Bridge Design, Master thesis, Kassel University, Delft, Netherlands, 2016.

J. Cao, X. Shao, L. Deng, Y. Gan, Static and fatigue behavior of short-headed studs embedded in a thin ultrahigh-performance concrete layer, *Journal of Bridge Engineering* 22 (2017) 04017005.

P. Szary, A. M. Roda, et al., Bridge resource program., Technical Report, Rutgers University. Center for Advanced Infrastructure & Transportation, 2013.

T. R. Schmitt, D. Darwin, Effect of material properties on cracking in bridge decks, *Journal of Bridge Engineering* 4 (1999) 8-13.

C. Schultz, P. R. Cunningham, J. Fan, S. A. Miller, Balancing the mechanical performance and environmental sustainability of fiber reinforced concrete, *Journal of Materials in Civil Engineering* TBD (2025).

Intergovernmental Panel on Climate Change, *Climate Change 2022 - Mitigation of Climate Change: Working Group III Contribution to the Sixth Assessment Report of the Intergovernmental Panel on Climate Change*, Cambridge University Press, 2022. doi:10.1017/9781009157926.013.

P. Colligan, E. Van Roijen, S. Kane, F. Moore, S. A. Miller, The unaccounted-for climate costs of materials, *Environmental Research Letters* 19 (2024) 114063.

K. Rennert, F. Errickson, B. C. Prest, L. Rennels, R. G. Newell, W. Pizer, C. Kingdon, J. Wingenroth, R. Cooke, B. Parthum, et al., Comprehensive evidence implies a higher social cost of CO₂, *Nature* 610 (2022) 687-692.

K. Cui, K. Liang, J. Chang, D. Lau, Investigation of the macro performance, mechanism, and durability of multiscale steel fiber reinforced low-carbon ecological uhpc, *Construction and Building Materials* 327 (2022) 126921.

X. Zhang, Z. Wu, J. Xie, X. Hu, C. Shi, Trends toward lower-carbon ultra-high performance concrete (uhpc)-a review, *Construction and Building Materials* 420 (2024) 135602.